Original Article

JCBFM

Journal of Cerebral Blood Flow & Metabolism
2016, Vol. 36(8) 1464–1476

DOI: 10.1177/0271678X15611137
jcbfm.sagepub.com
SAGE

Non-invasive tracking of CD4$^+$ T cells with a paramagnetic and fluorescent nanoparticle in brain ischemia

Wei-Na Jin[1,2], Xiaoxia Yang[1], Zhiguo Li[2], Minshu Li[1,2], Samuel Xiang-Yu Shi[2], Kristofer Wood[2], Qingwei Liu[2], Ying Fu[1], Wei Han[1], Yun Xu[3], Fu-Dong Shi[1,2] and Qiang Liu[1,2]

Abstract

Recent studies have demonstrated that lymphocytes play a key role in ischemic brain injury. However, there is still a lack of viable approaches to non-invasively track infiltrating lymphocytes and reveal their key spatiotemporal events in the inflamed central nervous system (CNS). Here we describe an in vivo imaging approach for sequential monitoring of brain-infiltrating CD4$^+$ T cells in experimental ischemic stroke. We show that magnetic resonance imaging (MRI) or Xenogen imaging combined with labeling of SPIO-Molday ION Rhodamine-B (MIRB) can be used to monitor the dynamics of CD4$^+$ T cells in a passive transfer model. MIRB-labeled CD4$^+$ T cells can be longitudinally visualized in the mouse brain and peripheral organs such as the spleen and liver after cerebral ischemia. Immunostaining of tissue sections showed similar kinetics of MIRB-labeled CD4$^+$ T cells when compared with in vivo observations. Our results demonstrated the use of MIRB coupled with in vivo imaging as a valid method to track CD4$^+$ T cells in ischemic brain injury. This approach will facilitate future investigations to identify the dynamics and key spatiotemporal events for brain-infiltrating lymphocytes in CNS inflammatory diseases.

Keywords

Ischemic stroke, lymphocytes, CD4$^+$ T cells, USPIO, In vivo imaging

Received 5 March 2015; Revised 3 July 2015; Accepted 6 July 2015

Introduction

Stroke is second only to cardiac ischemia as a leading cause of death worldwide. Following the abrupt disruption of the blood-brain-barrier (BBB), the massive influx of lymphocytes from the periphery into the ischemic brain orchestrates focal inflammatory responses and contributes to brain damage.[1–5] It has been documented that cell types most frequently infiltrating the postischemic brain include neutrophils, macrophages, and natural killer (NK) cells, followed by CD4$^+$ and CD8$^+$ T cell subsets.[3,5–7] Such cells, as seen within the infarcted and peri-infarcted areas of brain tissues from acute ischemic stroke patients and experimental ischemic stroke animals, are intimately involved in all stages of the ischemic cascade.[2,3,6,7] Among these cellular elements, CD4$^+$ T cells are a prominent lymphocyte subset with both beneficial and deleterious effects in ischemic brain injury.[2,3,6,8–12] Although the intriguing role of specific lymphocyte subsets, such as CD4$^+$ T cells, in ischemic brain injury is currently being elucidated via *ex vivo* approaches, extracting cells from the brain tissues is technically difficult and laborious. Moreover, these extracted cells may not consistently retain their physiological features after mechanical and chemical dissociations. Thus, it remains

[1]Departments of Neurology, Immunology, Radiology, Key Laboratory of Neurorepair and Regeneration, Tianjin and Ministry of Education, Tianjin Neurological Institute, Tianjin Medical University General Hospital, Tianjin, China
[2]Department of Neurology, Barrow Neurological Institute, St. Joseph's Hospital and Medical Center, Phoenix, AZ, USA
[3]Department of Neurology, Affiliated Drum Tower Hospital, Nanjing University Medical School; Jiangsu Key Laboratory for Molecular Medicine, Nanjing University Medical School, Nanjing, China

Corresponding author:
Qiang Liu, Tianjin Neurological Institute, Tianjin Medical University General Hospital, Tianjin 300052, China.
Email: qliu@tijmu.edu.cn

challenging to better understand the biological roles and dynamic changes of specific lymphocyte subsets in brain ischemia.[13]

The recent advances in imaging technologies including magnetic resonance image (MRI)-based immune cell tracking with superparamagnetic iron oxide (SPIO) nanoparticles have been applied in many types of diseases.[14–16] The SPIO nanoparticles strongly perturb the proximal magnetic field and produce a local signal loss consequently, and SPIO labeled cells appear as areas of negative contrast on T2 weighted MRI.[13,17,18] In addition, SPIO particles can be conjugated to fluorochromes, which enable the validation of in vivo MRI detection of cells by subsequent *ex vivo* assays. Molday ION Rhodamine B (MIRB) is a novel iron oxide-based SPIO of a size of 35 nm, which is labeled with the fluorescent dye Rhodamine B (Rh-B) and can be visualized by both MRI and biofluorescence imaging. This reagent has a proprietary coating that allows the particle to be taken up by cells without transfection agents. Reportedly, MIRB is non-toxic to mammalian cells and has a half-life in the range of weeks.[19] Yet, it remains unknown whether MIRB can be used as a valid tool to track specific subsets of brain-infiltrating lymphocytes in vivo in the context of ischemic stroke.

In this study, we choose to track $CD4^+$ T cells as an example of infiltrating lymphocytes in the post-ischemic brain. We showed that MIRB-labeled $CD4^+$ T cells can be successfully visualized via 7T-MRI coupled with Xenogen imaging and immunostaining in the CNS and periphery. Our results demonstrated the use of MIRB in conjunction with in vivo imaging as a promising approach to non-invasively monitor lymphocytes in neuroinflammation.

Materials and methods

Animals

Male C57BL/6 (B6) mice and $Rag2^{-/-}$ mice (two- to three-month-old, 23–25 g body weight) were purchased from Taconic (Taconic Biosciences). The mutant mice were back-crossed to the B6 background for 8–12 generations. Mice were housed in pathogen-free conditions at the animal facilities of the Barrow Neurological Institute, St. Joseph's Hospital and Medical Center (Phoenix, AZ) and the Tianjin Neurological Institute, Tianjin Medical University General Hospital (Tianjin, China). All animal experiments were performed in strict accordance with the recommendations of the Guide for the Care and Use of Laboratory Animals of the National Institutes of Health and in accordance with the ARRIVE (Animal Research: Reporting in vivo Experiments) guidelines. The protocol was approved by the Committee on the Ethics of Animal Experiments of Barrow Neurological Institute and Tianjin Neurological Institute. All surgeries were performed under isoflurane anesthesia.

$CD4^+$ T cell isolation, MIRB labeling and cell passive transfer

$CD4^+$ T cells were sorted from pooled splenocytes of C57BL/6 mice as previously described.[5,20,21] Briefly, cell suspensions from the spleens of C57BL/6 donor mice were enriched for $CD4^+$ T cells using magnetic-bead sorting system after staining with anti-CD4 microbeads ($CD4^+$ T cell isolation kit, Miltenyi Biotech, San Diego, CA, USA) and followed by cell sorting selection with the high-speed sort of FACSAria (BD Biosciences, San Jose, CA, USA). The purity of $CD4^+$ T cells (>99%) was confirmed with flow cytometry.

SPIO-Molday ION Rhodamine-B (MIRB, BioPhysics Assay Laboratory, Inc, Worcester, MA, USA) is an SPIO contrast agent. The SPIO component of MIRB is conjugated to Rhodamine-B (Rh-B) (2 flourophores per particle). The whole size of MIRB is ~35 nm. After cell sorting, sorted $CD4^+$ T cells were then incubated in RPMI culture medium with the presence of MIRB (at a concentration of 12.5 μg/ml) for 24 h *ex vivo* at 5% CO_2 and 37°C. Cells were maintained in RPMI 1640 plus 10% FBS (Invitrogen, Grand Island, NY, USA), L-glutamine (2 mM), IL-2 (10 μg/ml), penicillin (100 U/ml), and streptomycin (0.1 mg/ml). After incubation, cells underwent centrifugation (400 × *g*, 5 min) and were washed twice with PBS to remove extracellular MIRB.

To study the impact of MIRB labeling on the functions of $CD4^+$ T cells, $CD4^+$ T cells were cultured at 5% CO_2 and 37°C with or without MIRB labeling for 1–7 days. Labeling efficiency was determined by fluorescence microscopy and flow cytometry. A BrdU assay was conducted on unlabeled and labeled $CD4^+$ T cells according to the manufacturer's protocol. $CD4^+$ T cells were stimulated with anti-CD3 (3 mg/ml) and anti-CD28 (1 mg/ml) in 200 μl of complete RPMI at 37°C for 4 h following BrdU assay, to examine the effect of MIRB-labeling on cell proliferation (BrdU PE flow kit, BD Biosciences). The rate of Annexin V-positive apoptotic $CD4^+$ T cells was determined by flow cytometry at various time points after MIRB exposure (Annexin V–FITC apoptosis detection kit, BD Biosciences). The activation and functional status of the cells was determined by examining the expression of surface receptors for CD69 (H1.2F3), CD25 (PC61), and IL-2, together with intracellular IFN-γ (XMG1.2) using flow cytometry. All antibodies were purchased from BD or eBioscience. Flow cytometric measurements were performed on a FACSAria system (BD Biosciences) and analyzed using Flowjo 7.6 software (Informer Technologies, Walnut, CA, USA).

Before being transferred into $Rag2^{-/-}$ recipient mice (lacking T and B cells), the purity of MIRB-labeled or unlabeled $CD4^+$ T cells (~98%) was validated by the detection of $CD4^+$Rh-B^+ or $CD4^+$ T cells with flow cytometry as previously described.[5] Then, MIRB-labeled or unlabeled $CD4^+$ T cells were washed with PBS. Subsequently, 3×10^6 of either MIRB-labeled or unlabeled $CD4^+$ T cells were injected intravenously (i.v.) into the tail vein of $Rag2^{-/-}$ recipient mice. Immediately after transfer, the $Rag2^{-/-}$ recipients were subjected to sham or 60 min MCAO surgeries.

Middle cerebral artery occlusion (MCAO) procedure

$Rag2^{-/-}$ mice were subjected to a 60 min focal cerebral ischemia produced by transient intraluminal occlusion of middle cerebral artery (MCA) using a filament method as described previously.[5,20–22] MCA occlusion (MCAO) was performed under anesthesia by inhalation of 3.5% isoflurane and maintained by inhalation of 1.0–2.0% isoflurane in 70% N_2O and 30% O_2 by a face mask. A monofilament with rounded tip was used to induce focal cerebral ischemia for 60 min by occlusion of the right MCA. After 60 min of MCAO, the occluding filament was withdrawn into the common carotid artery to allow reperfusion. Sham control mice were subjected to the same surgical procedure, but the filament was not advanced far enough to occlude the MCA. 7T-MRI was employed to measure the infarct volume after MCAO (see the Neuroimaging section). Neurological deficit assessment was performed by experimenters blinded to the sham and MCAO groups as we previously described.[5,20–22] The rating scale was as follows: 0 = no deficit, 1 = failure to extend left forepaw, 2 = decreased grip strength of left forepaw, 3 = circling to left by pulling the tail, 4 = spontaneous circling, and 5 = dead. Following surgery, each mouse was assessed on a scale from 0 to 5 upon awakening, and only mice receiving a score of > 1 were included in this study. In all experiments, the mortality rate of $Rag2^{-/-}$ mice subjected to MCAO was ~7%.

Neuroimaging

All the scans were performed using a 7T small animal, 30 cm horizontal-bore magnet and BioSpec Avance III spectrometer (Bruker, Billerica, MA, USA). A 72 mm linear transmitter coil and mouse surface receiver coil were used for mouse brain imaging as previously described.[5,20,21] Mice were under anesthesia by inhalation of 3.5% isoflurane and maintained by inhalation of 1.0–2.0% isoflurane in 70% N_2O and 30% O_2 by a face mask. During MRI scan, the animal's respiration was continually monitored by a small animal monitoring and gating system (SA Instruments, Stoney Brook, NY, USA) via a pillow sensor positioned under the abdomen. Mice were placed on a heated circulating water blanket (Bruker, Billerica, MA, USA) to maintain normal body temperature (36–37°C). The T1-weighted images of the spleen were acquired by Fast Low Angle Shot (FLASH) sequence, as we did previously[5,20,21,23] (TR = 350 ms, TE = 3.795 ms, FOV 35.0 mm × 35.0 mm, matrix size = 256 × 256, slice thickness = 0.5 mm, TA = 1m7s). Axial 2D multi-slice T2-weighted images of the brain were acquired with fat-suppressed Rapid Acquisition with Relaxation Enhancement (RARE) sequence (TR = 4000 ms, effective TE = 60 ms, number of average = 4, FOV = 19.2 mm × 19.2 mm, matrix size = 192 × 192, slice thickness = 0.5 mm, TA = 6m24s). In vivo T2*-weighted images were acquired with FLASH sequence (number of slices = 29, TR 1000 ms, TE = 12.0 ms, number of average = 2, Flip angle = 45°, FOV = 19.2 mm × 19.2 mm, matrix size = 256 × 256, slice thickness = 0.5 mm, TA = 6m24s). In order to quantify MIRB signal, we scanned Multislice Gradient Echo (MGE) sequence and accordingly acquired T2*-map as well as R2* relaxation rates in the brain, spleen and liver as previously described.[24–26] For in vivo T2*-mapping, 10 gradient echoes were acquired (MGE: TR = 120 ms, echo time = 3.0, 6.0, 9.0, 12.0, 15.0, 18.0, 21.0, 24.0, 27.0, 30.0 ms, field of view = 35.0 mm × 35.0 mm, matrix = 128 × 128, slice thickness = 0.5 mm, flip angle 80°). T2* maps were generated by Bruker's built-in software, by fitting the T2* decayed signal curve along echo time series. R2* (R2* = 1/T2*) was used to quantify the signal intensity. The mean R2* values were measured within a region of interest (ROI) drawn by a blinded, experienced MR specialist. In the brain, ROIs were drawn around the individual dark spots in five consecutive slices on T2* map with the fixed size of 300 pixels per slice. In the spleen, the ROIs were drawn across all slices to include the entire spleen. In the liver, ROIs were drawn to cover the whole liver parenchyma excluding the major blood vessels across all slices. The MRI data were analyzed with Image J software (National Institutes of Health, MD, USA) as we previously reported.[5,21–23]

To track Rh-B fluorescence in the brain, biofluorescence images in live mice were captured using the Xenogen IVIS200 system (Caliper Life Sciences, MA, USA) for seven days following the transfer of MIRB-labeled $CD4^+$ T cells. After Xenogen imaging, the ROI tool was used to measure the intensity of the fluorescence on these images. Data were collected as photons per second per centimeter squared using the Living Image 4.0 software (Caliper Life Sciences, MA, USA).[5,20–22]

Histology stains

The immunohistochemistry staining was performed as previously described.[5,20–22,27] Briefly, immediately after

completion of $CD4^+$ T imaging by MRI, mice were euthanized. Brain, spleen and liver tissues were harvested and fixed in 4% paraformaldehyde, and then dehydrated with 15% and 30% sucrose. The tissues were embedded in OCT for preparation of frozen sections. The samples were cut to a thickness of 30 μm and blocked in 5% goat serum for 1 h at room temperature. Thereafter, tissue sections were incubated with anti-mouse CD4 (1:100, MT310, Santa Cruz Biotechnology, Dallas, TX, USA) primary antibody at 4°C overnight, and then incubated with FITC-conjugated goat anti-mouse secondary antibodies (1:2000, BD Bioscience) at room temperature for 1 h. Nuclei were co-stained with 4′,6-diamidino-2-phenylindole (DAPI, Abcam, Cambridge, MA, USA). Images were captured by a fluorescence microscopy (Olympus, model BX-61). After immunostaining, counts of labeled or unlabeled $CD4^+$ T cells were made by counting $CD4^+Rh\text{-}B^+$ or $CD4^+$ cells in the every tenth tissue section throughout the entire tissue block. Image analysis was performed using Image J software (National Institutes of Health, MD, USA).

Prussian blue staining was performed to verify the cellular uptake of the MIRB particles. After cell fixation, both the cultured MIRB-labeled $CD4^+$ T cells and tissue slices that contain MIRB-labeled $CD4^+$ T cells were incubated with working solution of Prussian blue staining reagent (reagent A: B = 1:1 v/v, BioPhysics Assay Laboratory, Inc.) and allowed to sit for 10 min at room temperature. The iron was stained blue and subsequently visualized by microscopy (Olympus, model BX-61).

Statistical analysis

Statistical analyses were performed using GraphPad Prism software. Two-tailed unpaired Student *t*-test was used to determine the significance of differences between two groups. One-way ANOVA followed by Tukey *post hoc* test was used for comparisons of three or more groups. Two-way ANOVA followed by Bonferroni post-tests was used for multiple comparisons. Pearson's correlation coefficient was used to measure the correlation between the extent of $CD4^+$ T cell infiltration and neurological deficits. Significance was set at $P < 0.05$. Data are shown as means ± SD.

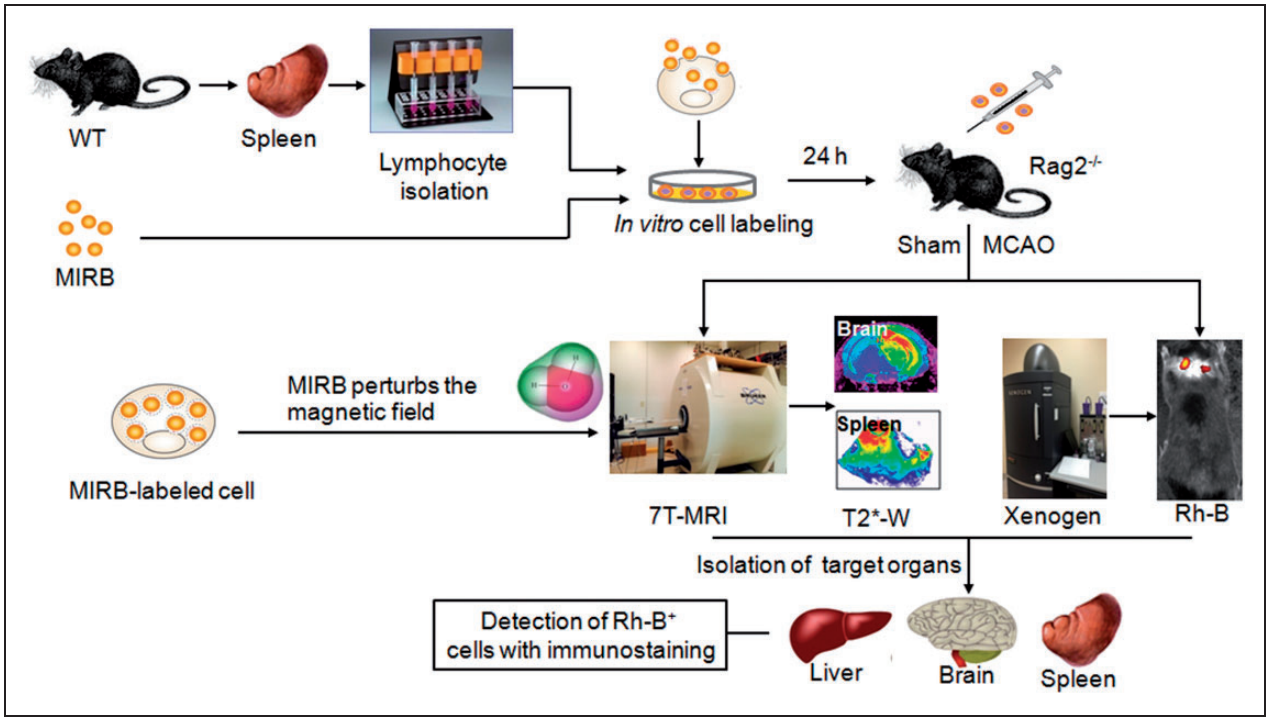

Figure 1. Schematic showing labeling of lymphocytes with MIRB and subsequent *in vivo* visualization. $CD4^+$ T cells were obtained from splenocytes of C57BL/6 mice. After in vitro incubation with MIRB for 24 h, $CD4^+Rh\text{-}B^+$ T cells were sorted and purified with FACS followed by subsequent passive transfer into $Rag2^{-/-}$ recipient mice (lack of T and B cells). After sham or 60 min of MCAO procedures with designated time of reperfusion, MIRB-labeled cells were sequentially visualized using 7T-MRI and Xenogen imaging. In separate groups of $Rag2^{-/-}$ mice that received MIRB-labeled $CD4^+$ T cells prior to sham or MCAO surgeries, brain, liver, and spleen sections were obtained from these animals after MRI scans and immunostained with CD4 specific antibody, and the images were captured by a fluorescence microscopy.

Results

Labeling of CD4$^+$ T cells with MIRB

The procedures for MIRB-labeling and detection of MIRB-labeled CD4$^+$ T cells were depicted in Figure 1. To label CD4$^+$ T cells with MIRB, we isolated CD4$^+$ T cells from splenocytes using magnetic-beads coupled with two rounds of sorting with FACS, which yielded highly purified CD4$^+$ T cells ($\geq$98%). CD4$^+$ T cells were then incubated with MIRB particles (12.5 μg/ml) for 24 h. Immunostaining results showed that Rhodamine B (Rh-B) positive cells are CD4$^+$ T cells (Figure 2a). Moreover, these CD4$^+$Rh-B$^+$ cells are also Prussian blue positive (Figure 2a). To quantify the efficiency of MIRB-labeling, MIRB-labeled CD4$^+$ T cells were cultured for up to seven days in vitro (DIV). Although the percentage of CD4$^+$Rh-B$^+$ T cells to the total number of CD4$^+$ T cells trended downward from 1 to 7 DIV, there was no statistical significance (Figure 2b) and >90% of CD4$^+$ T cells were still Rh-B$^+$ at 7 DIV (92.3 ± 2.1%). To obtain purified MIRB-labeled CD4$^+$ T cells for adoptive transfer studies, after cultured with MIRB for 24 h, CD4$^+$ T cells were then sorted twice with flow cytometry to gain a purity of ~98% (i.e. 98% of CD4$^+$ cells are CD4$^+$Rh-B$^+$, Figure 2c) prior to transfer.

MIRB labeling does not affect CD4$^+$ T cell survival and function

To understand whether MIRB internalization affects CD4$^+$ T cells, we examined the effects of MIRB labeling on the proliferation and apoptosis of CD4$^+$ T cells (Figure 3(a) to (d)). Results from BrdU and Annexin V assays showed that proliferation and apoptosis of CD4$^+$ T cells were not significantly altered by MIRB

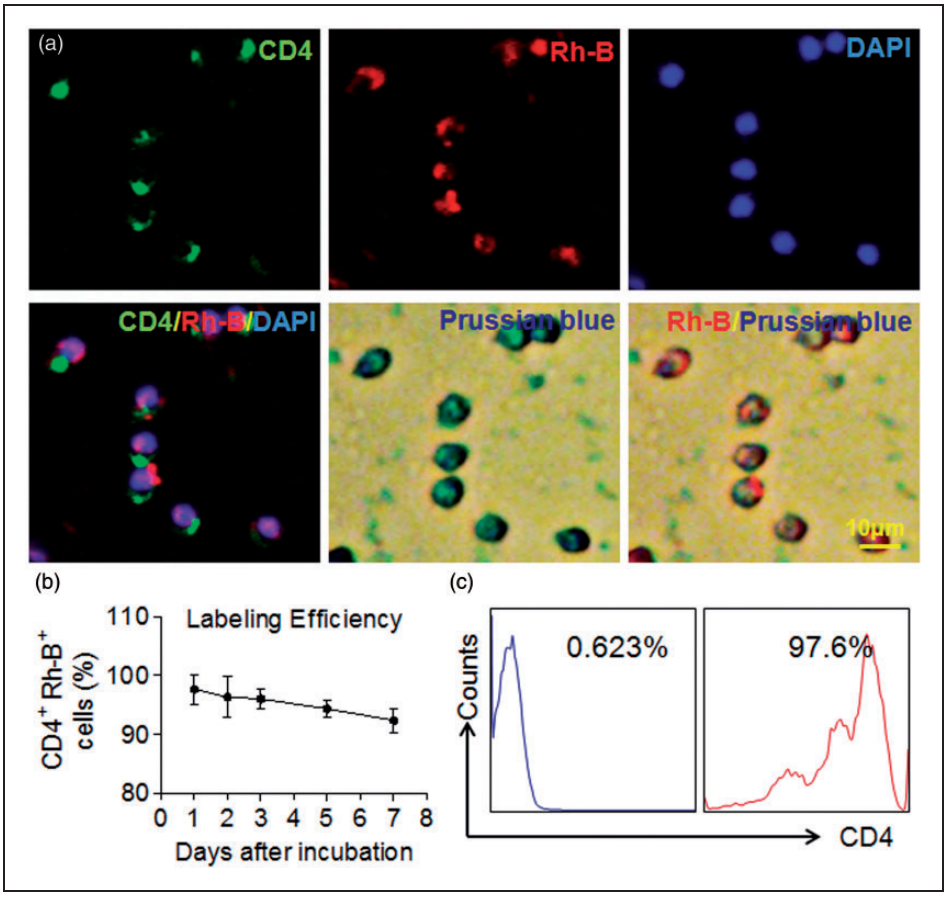

Figure 2. MIRB-labeling efficiency in purified CD4$^+$T cells. (a) FACS-sorted CD4$^+$T cells were incubated with MIRB (12.5 μg/ml) for 24 h. Representative immunofluorescence images and Prussian blue staining show uptake of MIRB particles by isolated CD4$^+$ T cells. CD4$^+$ T cells were stained by anti-CD4 antibody (green), red represents Rh-B$^+$ (red) cell, and the nucleus was stained with DAPI (blue). (b) Labeling efficiency of MIRB in CD4$^+$ T cells. MIRB labeled-CD4$^+$ T cells were cultured for seven days, flow cytometry analysis show CD4$^+$Rh-B$^+$ T cells percentage. (c). CD4$^+$Rh-B$^+$ T cells were purified with FACS sorting before i.v. passively transferred to Rag2$^{-/-}$ mice. Scale bar: 10 μm. Mean ± SD. Results were from at least three individual experiments.

internalization (Figure 3(a) and (b)). In addition, trypan blue exclusion assay showed that $CD4^+$ T cell viability was not altered by MIRB after 7 DIV (data not shown). Next, we sought to investigate whether MIRB alters the functional phenotype of $CD4^+$ T cells. After MIRB internalization, the expression of CD69, CD25, IL-2 and IFN-γ in $CD4^+$ T cells were not significantly changed compared to MIRB-untreated controls (Figure 3(c) and (d)). Altogether, these results suggest that MIRB internalization does not affect the survival or function of $CD4^+$ T cells.

To investigate the in vivo phenotype of $CD4^+$ T cells after adoptive transfer, flow cytometry was performed to assess the expression of apoptosis and functional markers of $CD4^+Rh\text{-}B^+$ cells isolated from the spleens of $Rag2^{-/-}$ recipient mice at day 1 after sham operations. As shown in Figure 3, the expression of an apoptosis marker (Annexin V), activation markers

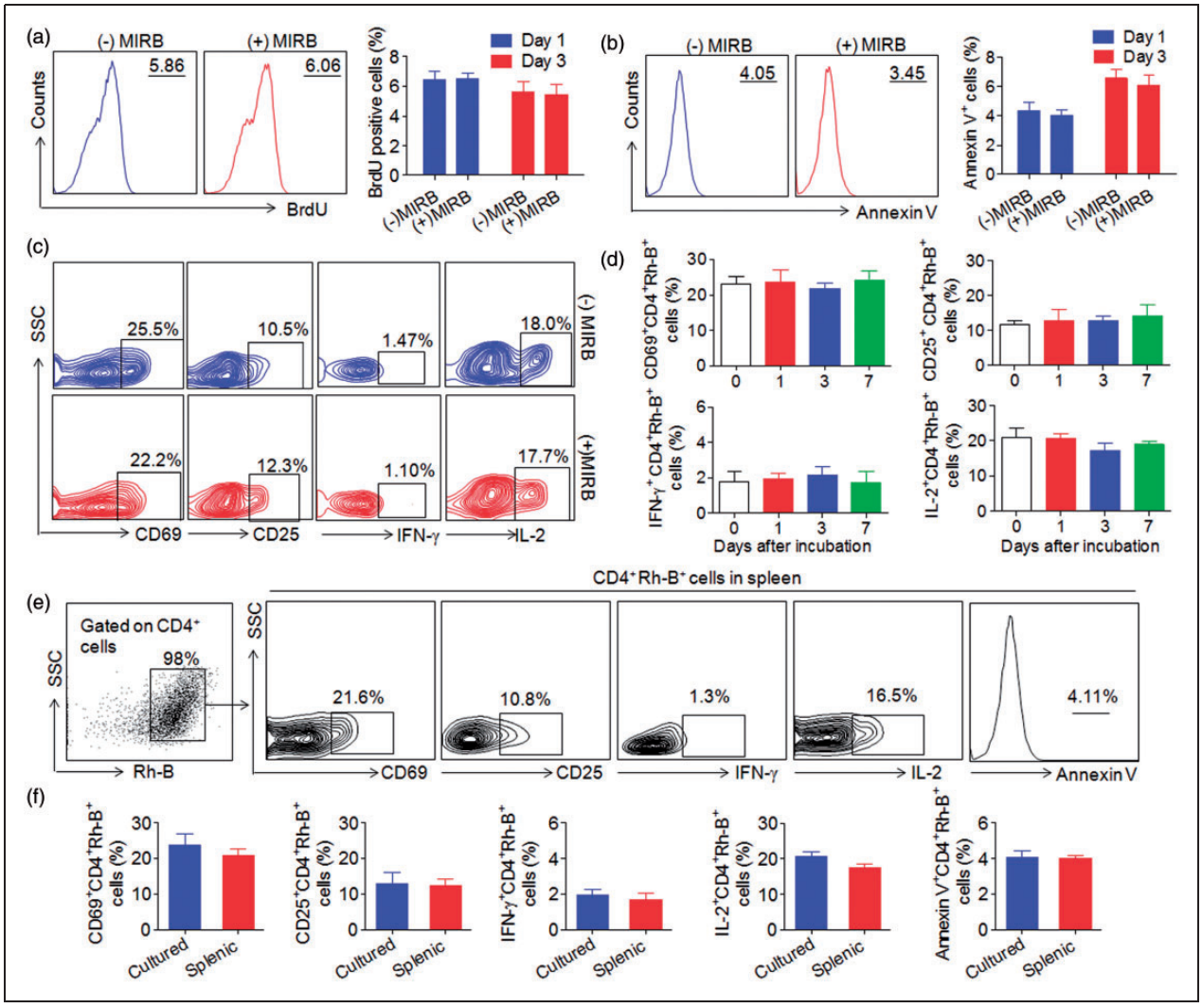

Figure 3. MIRB labeling has no effects on the phenotype and function of $CD4^+$T cells. (a) BrdU assay was performed to evaluate the impact of MIRB-labeling on the proliferation of $CD4^+$ T cells (left), and bar graph showed no significant effects (right). (b) Histograms of flow cytometry showed that MIRB-labeling does not affect apoptosis of $CD4^+$ T cells. (c) Flow cytometry analysis was performed to assess the effects of MIRB uptake on the expression of $CD4^+$ T cell surface and function markers (CD69, CD25, IFN-γ and IL-2). (d). The surface expression of $CD4^+$ T cell function markers was not altered after MIRB labeling until 7 days in vitro. (e) $Rag2^{-/-}$ mice received transfer of MIRB-labeled $CD4^+$ T cells prior to sham operations. At day 1 after sham operations, splenocytes were isolated from the spleens of $Rag2^{-/-}$ recipient mice. Flow cytometry analysis shows the gating strategy of $CD4^+Rh\text{-}B^+$ T cells and the expression of activation markers (CD69, CD25), cytokines (IL-2, IFN-γ), and an apoptosis marker (Annexin V). (f). Bar graphs summarize the expression of activation markers (CD69, CD25), cytokines (IL-2, IFN-γ), and an apoptosis marker (Annexin V) in $CD4^+Rh\text{-}B^+$ T cells isolated from the spleens of $Rag2^{-/-}$ recipient mice (splenic) or in $CD4^+Rh\text{-}B^+$ T cells under in vitro culture conditions (cultured). Mean ± SD. Results were from at least three individual experiments.

(CD69, CD25) and intercellular cytokines (IL-2, IFN-γ) in $CD4^+Rh\text{-}B^+$ T cells isolated from the spleen were comparable to those of $CD4^+Rh\text{-}B^+$ T cells in cultures (Figure 3(e) and (f)). These results suggest that the phenotype of MIRB-labeled $CD4^+$ T cells was not significantly altered after adoptive transfer.

Visualization of MIRB-labeled $CD4^+$ T cells in the ischemic brain

To visualize $CD4^+$ T cells in the ischemic brain, MIRB-labeled $CD4^+$ T cells were passively i.v. transferred to $Rag2^{-/-}$ mice (lack of T and B cells) followed by 60 min MCAO. MCAO produces a focal infarct lesion in the ipsilateral cortex, striatum and thalamus area. MCAO lesions can be detected as an apparent heterogeneous hyperintensive regions on T2 weighted MRI scans and MIRB signals were observed as hypointensive spots (Figure 4a). Additional T2*-weighted MRI scans were performed to acquire higher contrast images that could better reflect MIRB-induced signal loss on MRI scans (Figure 4a). A subsequent T2*-map was used to quantify the punctuate areas of signal loss (hypointensive spots of MIRB) in the ischemic brain over the time course of MCAO (Figure 4(b) and (c)). On day 1, we found MIRB signals in the infarct and peri-infarct areas, as

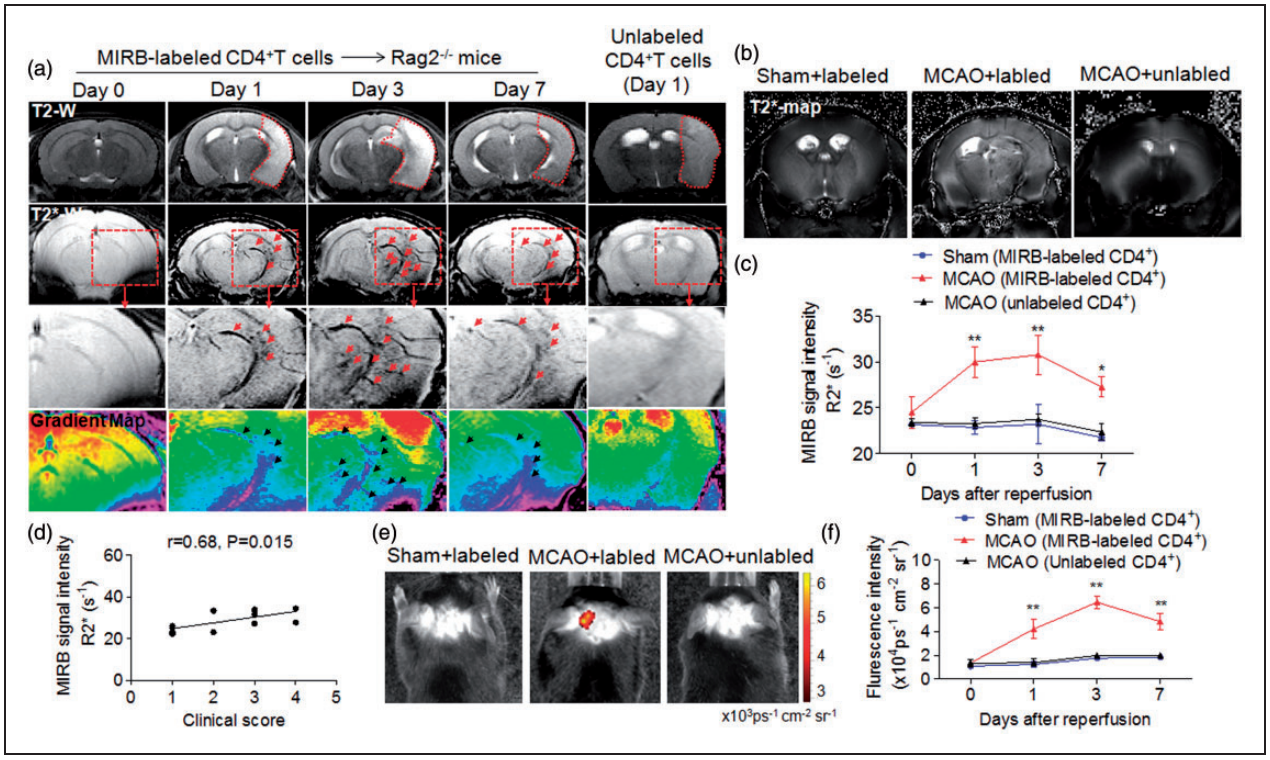

Figure 4. Visualization of MIRB-labeled $CD4^+$T cells in the ischemic brain. Three groups of mice underwent sequential MRI and Xenogen in vivo imaging, 12 $Rag2^{-/-}$ mice received 3×10^6 MIRB-labeled $CD4^+$ T cells prior to MCAO, 10 $Rag2^{-/-}$ mice received 3×10^6 unlabeled $CD4^+$ T cells prior to MCAO, and 10 $Rag2^{-/-}$ received 3×10^6 MIRB-labeled $CD4^+$ T cells before sham operation. Thereafter, these mice were longitudinally imaged at days 0, 1, 3 and 7 after surgeries. (a) Representative MRI images show brain lesion (T2-W) and hypointense spots of MIRB (T2*-W) in $Rag2^{-/-}$ mice receiving MIRB-labeled or unlabeled $CD4^+$ T cells at days 0, 1, 3 and 7 after surgeries. In T2-W image, regions surrounded with dotted red lines indicate areas of infarcts. Arrows in T2*-W image and gradient map indicate hypointensive spots of MIRB. (b) MRI images show hypointensive spots of MIRB in T2*- map in $Rag2^{-/-}$ mice that received MIRB-labeled or unlabeled $CD4^+$ T cells at day 1 after sham or MCAO surgeries. (c) Quantifications of the punctuate areas of signal loss (hypointensive spots of MIRB) were shown until seven days after surgeries. $F_{2,\ 116} = 7.73$, Sham (MIRB-labeled) *vs.* MCAO (MIRB-labeled), $P < 0.01$ at day 1 and 3, $P < 0.05$ at day 7. (d). Pearson correlation coefficient was used to measure the correlation between the intensity of dark spots seen on R2* map of MRI and neurodeficit scores in 12 $Rag2^{-/-}$ mice that received 3×10^6 MIRB-labeled $CD4^+$ T cells and underwent MCAO. The signal intensity of dark spots in the ischemic brain, i.e. magnitude of CD4 + T cell infiltration, correlates with the neurodeficit scores at day 1 after MCAO ($r = 0.68$; $P = 0.015$). (e) Representative Xenogen in vivo images show Rh-B fluorescence in $Rag2^{-/-}$ mice that received MIRB-labeled $CD4^+$ T cells before sham surgery, unlabeled $CD4^+$ T cells before MCAO, or MIRB-labeled $CD4^+$ T cells before MCAO. (f). Quantification of Rh-B fluorescence in $Rag2^{-/-}$ mice at the indicated time points after surgeries. $F_{2,\ 116} = 8.544$, Sham (MIRB-labeled) *vs.* MCAO (MIRB-labeled), $P < 0.01$ at days 1, 3 and 7. The results are representative of three separate experiments. Mean ± SD, *$P < 0.05$; **$P < 0.01$.

well as in the ipsilateral ventricular areas (Figure 4(a) to (c)). In particular, MIRB signals were detected primarily within the striatum and thalamus regions, which are reported to be the ischemic core in MCAO mice.[22,28] Later, until day 7, MIRB signals were persistently visualized and mainly detected within the cortical and lateral posterior nucleus, which are regions of delayed, progressive neuronal death, or an ischemic penumbra[28] (Figure 4a). In contrast, we did not detect notable hypointensive dots in Rag2$^{-/-}$ mice that received unlabeled CD4^{+} T cells and underwent MCAO surgery suggesting that the hypointensive spots seen in MCAO mice were not caused by microbleeds (Figure 4a). To test whether the extent of CD4^{+} T cell infiltration correlates to disease outcome, we examined the association between the intensity of dark spots seen on an MRI R2* map and the clinical score of neurodeficits in Rag2$^{-/-}$ mice that received MIRB-labeled CD4^{+} T cells and underwent MCAO surgery. Consistent with previous findings that show a detrimental role of CD4^{+} T cells in the early phase of stroke,[9,10] we found that higher intensity of dark spots in the ischemic brain, i.e. magnitude of CD4^{+} T cell infiltration, correlates with worse neurodeficit scores in these mice (Figure 4d).

To complement the MRI approach, Xenogen fluorescence imaging was utilized to capture Rh-B signal in the ischemic brain of the same groups of animals after MRI scans. In line with the observations of MRI scans,

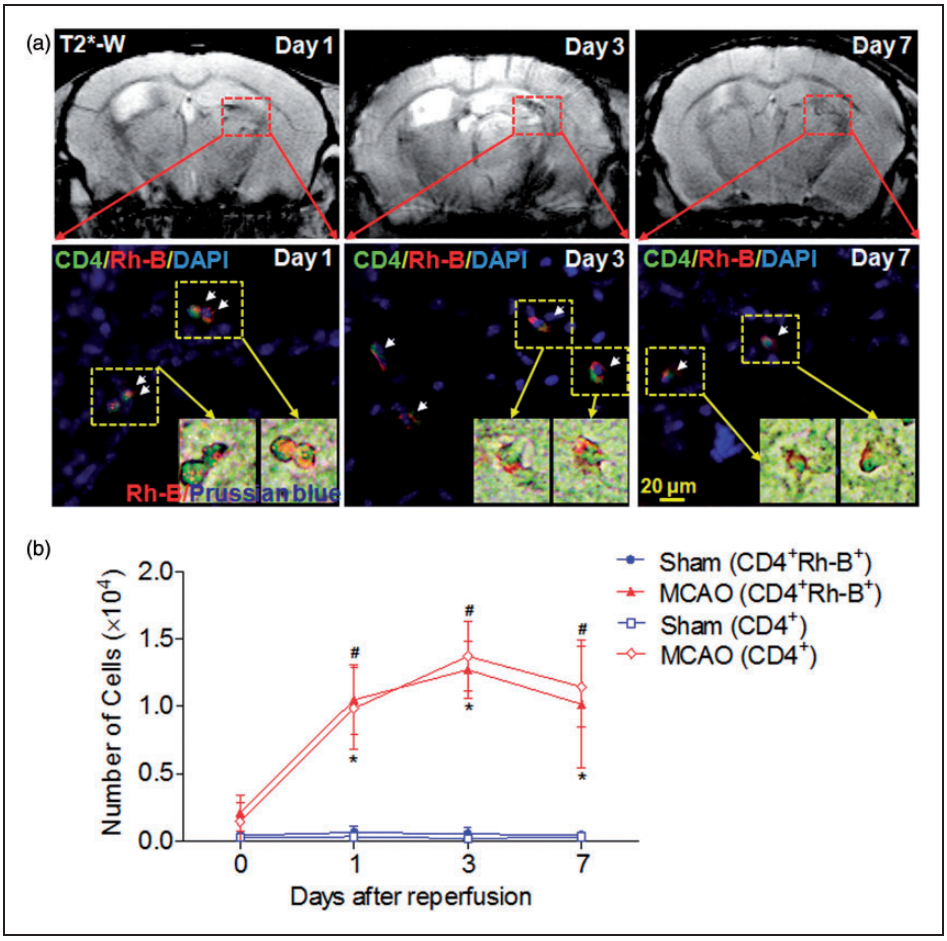

Figure 5. Immunostaining of MIRB-labeled CD4^{+} T cells in the ischemic brain. For histological staining, separate groups of Rag2$^{-/-}$ mice were i.v. transferred with 3×10^{6} MIRB-labeled CD4^{+} T cells prior to sham or MCAO surgeries. After MRI scans at 0, 1, 3, 7 post-surgeries, Rag2$^{-/-}$ mice were sacrificed and brain sections were stained with Prussian blue and CD4^{+} antibody to quantify CD4^{+}Rh-B^{+} T or CD4^{+} T cells. (a) Representative images show CD4^{+}Rh-B^{+} T cells in brain sections until seven days after MCAO. Green: CD4, red: Rh-B, and blue: DAPI. Prussian blue staining shows iron particles in CD4^{+}Rh-B^{+} T cells. (b) Quantification of brain-infiltrating CD4^{+} T cells and CD4^{+}Rh-B^{+} T cells in the whole brain tissue until seven days after MCAO or sham operations. $F_{3,64} = 7.57$; Sham (CD4^{+}Rh-B^{+}) *vs.* MCAO (CD4^{+}Rh-B^{+}), $P < 0.05$ at days 1, 3 and 7; Sham (CD4^{+}) *vs.* MCAO (CD4^{+}), $P < 0.05$ at days 1, 3 and 7. Scale bar: 20 μm. Data were from five mice per group. The results are representative of three separate experiments. Mean ± SD, $^{*}P < 0.05$, brain-infiltrating CD4^{+}Rh-B^{+} T cells in MCAO *vs.* sham control; $^{\#}P < 0.05$, brain-infiltrating CD4^{+} T cells in MCAO *vs.* sham control.

we found that the fluorescence of Rh-B can be visualized starting from day 1 after MCAO, and persist at least until day 7 with similar dynamics relative to MRI observations (Figure 4(e) and (f)).

To confirm in vivo findings with MRI/Xenogen, we used separate groups of animals for histology studies. After in vivo imaging with MRI/Xenogen, we sacrificed MCAO mice that received MIRB-labeled $CD4^+$ T cells and immunostained the brain sections with anti-CD4 antibody. Again, we found similar dynamics of infiltrating $CD4^+Rh\ B^+$ cells (Figure 5(a) and (b)). To further validate the presence of MIRB-labeled cells in the ischemic brain, we performed Prussian blue staining. We found that $Rh\text{-}B^+$ cells are indeed Prussian blue positive in the brain sections from MCAO mice (Figure 5a). To evaluate the potential impact of T cell proliferation on signal dilution, we counted $CD4^+$ and $CD4^+Rh\text{-}B^+$ cells in immunostained tissue sections. As shown in Figure 5(b), the dynamics of the total number of $CD4^+$ T cells was similar to those of $CD4^+Rh\text{-}B^+$ T cells. Therefore, these results together show the successful monitoring of MIRB-labeled $CD4^+$ T cells in vivo in the ischemic brain.

Visualization of MIRB-labeled $CD4^+$ T cells in the periphery

To visualize and characterize the kinetics of $CD4^+$ T cells in the periphery, we imaged MIRB-labeled $CD4^+$ T cells in the spleen and liver of $Rag2^{-/-}$ recipients. Prior to MCAO induction, MIRB-labeled $CD4^+$ T cells were identified as hypointense signals on MRI images in the periphery, mainly in the spleen and liver (Figure 6). In the spleen, MIRB signal intensity (the punctuate areas of signal loss) declined within the first 24 h after MCAO, reached the nadir on day 3, and became comparable with the sham-operated controls on day 7 (Figure 6(a) and (b)). In contrast, MIRB signal intensity fluctuated in the liver after MCAO,

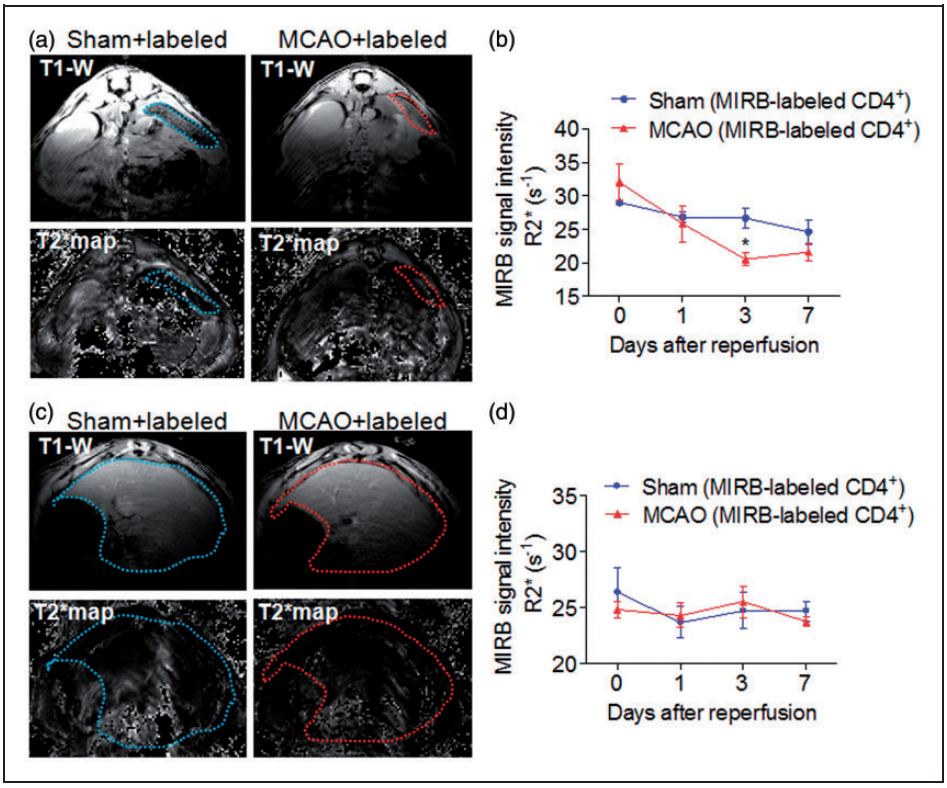

Figure 6. Visualization of MIRB-labeled $CD4^+$T cells in the periphery. 3×10^6 MIRB-labeled $CD4^+$ T cells were i.v. transferred into $Rag2^{-/-}$ mice prior to sham or MCAO surgeries. Animals were imaged until day 7 after surgeries. (a) Representative MRI images show spleen size (T1-W) and hypointense spots of MIRB in T2*-map at day 1 after sham or MCAO surgeries. Dotted lines surrounding area showed the area of spleen. (b) Quantification of the MIRB signal intensity (loss of signal) in spleen. The direct measurement of the mean R2* value was used for displaying and quantifying the hypointense spots of MIRB in the spleen. $F_{1,\ 80} = 6.465$, Sham (MIRB-labeled) *vs.* MCAO (MIRB-labeled), $P < 0.05$ at day 3. (c) MRI images show liver structure (T1-W) and the hypointense spots of MIRB (T2*-map). Regions surrounded with dotted lines show the outline of liver. (d) Quantification of the MIRB signal intensity (loss of signal) in liver. Results were from 22 $Rag2^{-/-}$ mice (12 MCAO mice that received MIRB-labeled $CD4^+$ T cells; 10 sham controls that received MIRB-labeled $CD4^+$ T cells). The results are representative of three separate experiments. Mean ± SD, $^*P < 0.05$; $^{**}P < 0.01$.

but remained comparable to those in sham controls (Figure 6(c) and (d)). To confirm in vivo findings with MRI, we used separate groups of animals for histology studies. After in vivo imaging with MRI, we performed immunostaining in these mice and found that the dynamic changes of $CD4^+Rh\text{-}B^+$ cells in the spleen and liver were comparable to those seen via MRI (Figure 7(a) to (d)). In addition, the dynamics of $CD4^+Rh\text{-}B^+$ cells were similar to those of $CD4^+$ T cells in the spleen and liver (Figure 7(b) and (d)), suggesting that the decline of MIRB signals correlates with the reduction in total counts of $CD4^+$ T cells. Together, these results demonstrate the different dynamics of $CD4^+$ T cells in the spleen and liver following brain ischemia.

Discussion

Here, we demonstrate a non-invasive method for sequential visualization of $CD4^+$ T cells with high magnetic-field MRI and Xenogen biofluorescence in vivo imaging using MIRB, a paramagnetic and fluorescent nanoparticle. The presence of MIRB-labeled $CD4^+$ T cells in the CNS was validated via *post hoc* histology staining. This method allowed us to successfully track lymphocytes in a live animal brain, spleen and liver for days. To our knowledge, this is the first report of sequentially monitoring a single lymphocyte subset during brain ischemia via in vivo imaging techniques, i.e. MRI and Xenogen imaging.

The use of MRI/Xenogen with MIRB to track immune cells has several advantages over other imaging approaches. The use of MRI/Xenogen combines both non-invasiveness and durability, which allows for the use of non-radioactive materials to perform long-term tracking of cells in vivo. Importantly, pervious single cell tracking approaches with SPIO could not assure that all cells are successfully labeled before transfer, because these approaches cannot exclude cells that have minimal or insufficient taken up SPIO for

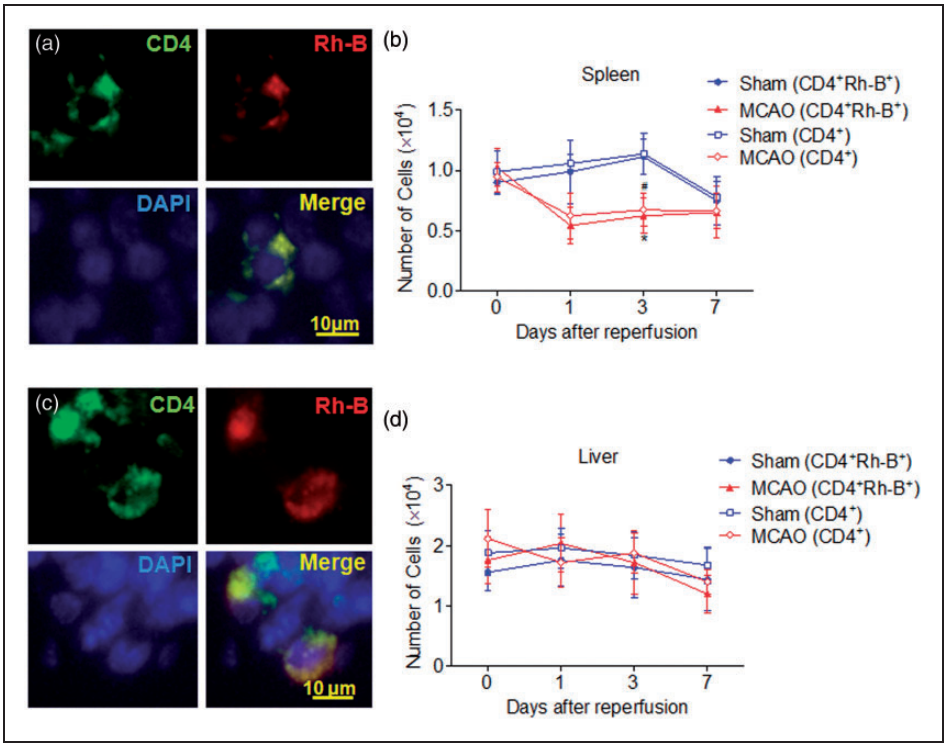

Figure 7. Immunostaining of MIRB-labeled $CD4^+$ T cells in the periphery. For histological staining, separate groups of $Rag2^{-/-}$ mice received i.v. transfer of 3×10^6 MIRB-labeled $CD4^+$ T cells prior to sham or MCAO surgeries. After MRI scans at 0, 1, 3, 7 post-surgeries, $Rag2^{-/-}$ mice were sacrificed and sections of spleen and liver tissues were stained with CD4 antibody, and then imaged with fluorescence microscopy. Green: CD4, red: Rh-B, and blue: DAPI. Representative images show $CD4^+Rh\text{-}B^+$ T cells in the spleen (a) and liver (c) tissue sections. Quantification of $CD4^+Rh\text{-}B^+$ cells with $CD4^+$ cells in the entire spleen (b) and liver (d) tissues after MCAO and sham operations. Spleen: $F_{3,64} = 8.873$; Sham ($CD4^+Rh\text{-}B^+$) *vs.* MCAO ($CD4^+Rh\text{-}B^+$), $P < 0.05$ at day 3; Sham ($CD4^+$) *vs.* MCAO ($CD4^+$), $P < 0.05$ at day 3. Scale bar: 10 μm. Data were from five mice per group. The results are representative of three separate experiments. Mean ± SD, $^*P < 0.05$; $^{**}P < 0.01$. $^*P < 0.05$, splenic $CD4^+Rh\text{-}B^+$ T cells in MCAO *vs.* sham control; $^{\#}P < 0.05$, splenic $CD4^+$ T cells in MCAO *vs.* sham control.

detection.[29–31] MIRB contains an Rh-B component, which can be coupled with FACS sorting to ensure the successful labeling of $CD4^+$ T cells (>99%) prior to transfer. Moreover, Rh-B allows the detection of labeled cells with histological or flow cytometry-based approaches as *post hoc* analysis to verify the presence of labeled $CD4^+$ T cells in the ischemic brain and periphery organs. Therefore, our present method is also superior in that it can fully detect all these purified cells in vivo after transfer. Although we cannot directly tell the absolute number of labeled cells based on MRI/Xenogen images, this technique allows us to sequentially monitor the dynamics of $CD4^+$ T cells in a single animal across the time course of ischemic stroke. This approach may facilitate a better understanding of the role of $CD4^+$ T cells in stroke pathogenesis. In addition, this approach can be also useful for tracking transferred lymphocytes in immunotherapy studies.

It is notable that the ideal cell-labeling protocols used for imaging cannot substantially alter the phenotype and function of the target cells.[13,32] Although according to a few studies SPIO labeling may have an impact on target cells to some extent,[33] most studies suggest that SPIO labeling has no significant effect on the phenotype and function of target cells.[13,17,29,30] For example, one recent report demonstrated that cytokine production, expression of surface markers, migratory capacity and antigen presentation did not differ in SPIO-labeled DCs as compared with unlabeled DCs.[34] Additionally, several iron oxide nanoparticles have been approved by the FDA and are already available for clinical use (ferumoxide, ferumoxytol, and ferucarbotran), which suggests that in vivo tracking with SPIO is safe and promising for clinical translation.[24] Unlike many other particles used to track immune cells, MIRB can be taken up by lymphocytes without transfection agents.[19,35] In the present study, we found that $CD4^+$ T cells can be effectively labeled with MIRB without altering $CD4^+$ T cell survival or function both in vitro and in vivo (Figure 3). In addition, we found that MIRB taken-up was retained in most $CD4^+$ T cells either in vitro or in vivo after they migrate into the ischemic brain, at least during the tested period of time. These findings support the notion that MIRB is non-toxic and can be retained in $CD4^+$ T cells. These features allow MIRB to be used as a suitable particle to track lymphocytes in vivo.

We found an increase of hypointense spots in the ischemic brain of $Rag2^{-/-}$ mice that received MIRB-labeled $CD4^+$ T cells after brain ischemia. Together with observations via Xenogen imaging and additional post hoc pathological analysis of labeled $CD4^+$ T cells, this finding suggests homing of labeled $CD4^+$ T cells into the ischemic brain following the disruption of the BBB due to cerebral ischemia. In addition, we observed a reduction in the number of labeled $CD4^+$ T cells in the spleen after MCAO, while the number of labeled $CD4^+$ T in the liver was relatively constant. This finding is consistent with previous publications that show ischemic brain injury can lead to reduced counts of $CD4^+$ T cells in the spleen.[36–38] Therefore, we postulate that brain ischemia-induced migration or splenic release of these labeled $CD4^+$ T cells from the spleen into other compartments could be responsible for the decline of $CD4^+$Rh-B^+ cells in the spleen. Nevertheless, other possibilities cannot be excluded, and the underlying mechanisms warrant future investigations.

Previous reports have demonstrated $CD4^+$ T cells as a key contributor to ischemic brain injury, especially in acute stroke.[2,3,10,11] In this study, we found that MCAO mice with more brain-infiltrating $CD4^+$ T cells, as manifested by more hypointensive dots or stronger biofluorescence intensity in the brain, were associated with worse clinical scores (Figure 4d). These findings are consistent with these previous reports and support a detrimental role of $CD4^+$ T in the early phase of ischemic brain injury.

Our findings are also consistent with current knowledge regarding the dynamics of infiltrating $CD4^+$ T cells obtained via *ex vivo* approaches including flow cytometry and immunostaining in brain ischemia.[1–3,6,7,13,39] Similarly, these studies showed infiltration of $CD4^+$ T cells starting from 24 h after MCAO with subsequent accumulation in the ischemic hemisphere. However, these conventional approaches cannot easily survey the whole brain longitudinally in live animals, and thus hinders further understanding of their biological function in vivo. Our current method can thus be a powerful tool that can not only confirm conclusions from the *ex vivo* studies, but also extend these findings to in vivo whole-brain tracking of these cellular infiltrates.[32]

To test the potential impact of T cell proliferation on signal dilution, we counted $CD4^+$ and $CD4^+$Rh-B^+ cells in immunostained tissue sections. We noticed that the dynamics of the total number of $CD4^+$ T cells resemble those in $CD4^+$Rh-B^+ T cells. Even at day 7 after brain ischemia, the majority of $CD4^+$ cells (~92.3%) remain $CD4^+$Rh-B^+. These results suggest that the decline of MIRB signals both in MRI and fluorescence correlates to the reduction in total counts of $CD4^+$ T cells observed in immunohistological sections.

Of note, although we found Prussian $blue^+$ cells in the brain areas that have dark spots on MRI images, we cannot conclude that the Prussian $blue^+$ cells are exactly the dark spots on MRI images because the pathology section may not be from exactly the same level shown on the MRI images. Nevertheless, these

findings can at least support the presence of MIRB-labeled cells in the corresponding brain area. We found some hypointense spots which are seen temporarily in MRI scan but disappear from the ischemic brain on day 7 after MCAO. We believe that this phenomenon may be caused by cell movement rather than cell lysis. This is because hypointense spots would still exist in adjacent areas after cell lysis due to the uptake by CNS phagocytes. However, these disappearing spots barely reemerge in adjacent areas. Unfortunately, it is technically challenging to verify whether an individual spot on MRI image is the same spot that migrated from another section, because the slice thickness is relatively large in MRI and Xenogen imaging does not have sufficient resolution. Thus, the disappearance of these hypointense spots may potentially result from cell migration or other unknown processes, which requires further investigation.

To characterize the dynamics of $CD4^+$ T cells in the periphery, we imaged the MIRB signals in the spleen and liver after MCAO. We attempted to find hypointense signals using T2-weighted and T2*-weighted images in the spleen and liver. However, the interpretation of the signal loss is difficult because of artifacts due to air–tissue interfaces and the inhomogeneities of peripheral tissues. Since the relaxation rate maps can provide quantification of the attenuated signal intensity, we used T2*-map sequence to quantify MIRB-labeled $CD4^+$ T cells in peripheral organs as reported by many other groups.[16,24] It is notable that the blood flow in the vessel, magnetic field inhomogeneity due to poor shimming, and air–tissue interfaces could all complicate the MRI images. On the other hand, Xenogen imaging also has limitations regarding the detection of biofluorescence signals in peripheral deep tissues and therefore renders it difficult to image MIRB-labeled cells in peripheral organs. Therefore, future optimization is needed to improve the detection of MIRB-labeled cells in the periphery.

Conclusions

In conclusion, we demonstrated the use of MIRB coupled with MRI/Xenogen imaging as a viable approach to non-invasively track $CD4^+$ T cells in vivo during brain ischemia. This approach may facilitate further investigations regarding temporal and spatial changes of infiltrating lymphocytes in neuroinflammation. When combined with *post hoc* pathological analysis, this non-invasive single-cell monitoring method may be useful for longitudinally correlating the behavior of immune cells to the curable areas and irreversibly damaged ones, and ultimately helps to resolve how lymphocytes may act in CNS inflammatory diseases.

Funding

This study was supported in part by the National Basic Research Program of China (grant no. 2013CB966900), the National Key-Project of Clinical Neurology, the National Science Foundation of China (grant nos 81230028, 81301044, 81471535), American Heart Association (grant no. GRNT18970031), National Institutes of Health Grants R01AI083294, the PhD Programs Foundation of Ministry of Education of China (grant no. 20121202120007), and the Tianjin Education Commission Foundation (grant nos 20120116 and 14JCYBJC42000).

Declaration of conflicting interests

The author(s) declared no potential conflicts of interest with respect to the research, authorship, and/or publication of this article.

Authors' contributions

W-NJ acquired, analyzed and interpreted the data, drafted the manuscript, made critical revision of the manuscript, acquired funding of the study. XY made critical revision of the manuscript. ZL and ML acquired the data. SX-YS analyzed and interpreted the data. KW analyzed and interpreted the data and edited the language of manuscript. QL analyzed and interpreted the data and made critical revision of the manuscript. YF and WH analyzed and interpreted the data. YX analyzed and interpreted the data and made critical revision of the manuscript. F-DS formulated the study concept, designed the study, and acquired funding of the study. QL formulated the study concept, designed the study, drafted the manuscript, made critical revision of the manuscript, and acquired funding of the study.

References

1. Gelderblom M, Leypoldt F, Steinbach K, et al. Temporal and spatial dynamics of cerebral immune cell accumulation in stroke. *Stroke* 2009; 40: 1849–1857.
2. Iadecola C and Anrather J. The immunology of stroke: From mechanisms to translation. *Nat Med* 2011; 17: 796–808.
3. Chamorro A, Meisel A, Planas AM, et al. The immunology of acute stroke. *Nat Rev Neurol* 2012; 8: 401–410.
4. Fu Y, Zhang N, Ren L, et al. Impact of an immune modulator fingolimod on acute ischemic stroke. *Proc Natl Acad Sci U S A* 2014; 111: 18315–18320.
5. Gan Y, Liu Q, Wu W, et al. Ischemic neurons recruit natural killer cells that accelerate brain infarction. *Proc Natl Acad Sci U S A* 2014; 111: 2704–2709.
6. Kamel H and Iadecola C. Brain–immune interactions and ischemic stroke: Clinical implications. *Arch Neurol* 2012; 69: 576–581.
7. Becker KJ. Activation of immune responses to brain antigens after stroke. *J Neurochem* 2012; 123: 148–155.
8. Liesz A, Suri-Payer E, Veltkamp C, et al. Regulatory t cells are key cerebroprotective immunomodulators in acute experimental stroke. *Nat Med* 2009; 15: 192–199.

9. Yilmaz G, Arumugam TV, Stokes KY, et al. Role of t lymphocytes and interferon-gamma in ischemic stroke. *Circulation* 2006; 113: 2105–2112.
10. Kleinschnitz C, Schwab N, Kraft P, et al. Early detrimental t-cell effects in experimental cerebral ischemia are neither related to adaptive immunity nor thrombus formation. *Blood* 2010; 115: 3835–3842.
11. Clarkson BD, Ling C, Shi Y, et al. T cell-derived interleukin (il)-21 promotes brain injury following stroke in mice. *J Exp Med* 2014; 211: 595–604.
12. Shichita T, Sugiyama Y, Ooboshi H, et al. Pivotal role of cerebral interleukin-17-producing gammadeltat cells in the delayed phase of ischemic brain injury. *Nat Med* 2009; 15: 946–950.
13. Ahrens ET and Bulte JW. Tracking immune cells in vivo using magnetic resonance imaging. *Nat Rev Immunol* 2013; 13: 755–763.
14. Anderson SA, Shukaliak-Quandt J, Jordan EK, et al. Magnetic resonance imaging of labeled t-cells in a mouse model of multiple sclerosis. *Ann Neurol* 2004; 55: 654–659.
15. Moore A, Sun PZ, Cory D, et al. Mri of insulitis in autoimmune diabetes. *Magn Reson Med* 2002; 47: 751–758.
16. Kircher MF, Allport JR, Graves EE, et al. In vivo high resolution three-dimensional imaging of antigen-specific cytotoxic t-lymphocyte trafficking to tumors. *Cancer Res* 2003; 63: 6838–6846.
17. Weinstein JS, Varallyay CG, Dosa E, et al. Superparamagnetic iron oxide nanoparticles: Diagnostic magnetic resonance imaging and potential therapeutic applications in neurooncology and central nervous system inflammatory pathologies, a review. *J Cereb Blood Flow Metab* 2010; 30: 15–35.
18. Oude Engberink RD, Blezer EL, Hoff EI, et al. Mri of monocyte infiltration in an animal model of neuroinflammation using spio-labeled monocytes or free uspio. *J Cereb Blood Flow Metab* 2008; 28: 841–851.
19. Shen WB, Plachez C, Chan A, et al. Human neural progenitor cells retain viability, phenotype, proliferation, and lineage differentiation when labeled with a novel iron oxide nanoparticle, molday ion rhodamine b. *Int J Nanomed* 2013; 8: 4593–4600.
20. Hao J, Liu R, Piao W, et al. Central nervous system (cns)-resident natural killer cells suppress th17 responses and cns autoimmune pathology. *J Exp Med* 2010; 207: 1907–1921.
21. Liu Q, Tang Z, Gan Y, et al. Genetic deficiency of beta2-containing nicotinic receptors attenuates brain injury in ischemic stroke. *Neuroscience* 2014; 256: 170–177.
22. Tang Z, Gan Y, Liu Q, et al. Cx3cr1 deficiency suppresses activation and neurotoxicity of microglia/macrophage in experimental ischemic stroke. *J Neuroinflam* 2014; 11: 26.
23. Bell JC, Liu Q, Gan Y, et al. Visualization of inflammation and demyelination in 2d2 transgenic mice with rodent mri. *J Neuroimmunol* 2013; 264: 35–40.
24. Daldrup-Link HE, Meier R, Rudelius M, et al. In vivo tracking of genetically engineered, anti-her2/neu directed natural killer cells to her2/neu positive mammary tumors with magnetic resonance imaging. *Eur Radiol* 2005; 15: 4–13.
25. Sheu AY, Zhang Z, Omary RA, et al. Mri-monitored transcatheter intra-arterial delivery of spio-labeled natural killer cells to hepatocellular carcinoma: Preclinical studies in a rodent model. *Invest Radiol* 2013; 48: 492–499.
26. Wang Q, Li K, Quan Q, et al. R2* and r2 mapping for quantifying recruitment of superparamagnetic iron oxide-tagged endothelial progenitor cells to injured liver: Tracking in vitro and in vivo. *Int J Nanomed* 2014; 9: 1815–1822.
27. Shi FD and Van Kaer L. Reciprocal regulation between natural killer cells and autoreactive t cells. *Nat Rev Immunol* 2006; 6: 751–760.
28. Carmichael ST. Rodent models of focal stroke: Size, mechanism, and purpose. *NeuroRx* 2005; 2: 396–409.
29. Sta Maria NS, Barnes SR and Jacobs RE. In vivo monitoring of natural killer cell trafficking during tumor immunotherapy. *Magn Reson Insight* 2014; 7: 15–21.
30. Mori Y, Chen T, Fujisawa T, et al. From cartoon to real time mri: In vivo monitoring of phagocyte migration in mouse brain. *Sci Rep* 2014; 4: 6997.
31. Dekaban GA, Hamilton AM, Fink CA, et al. Tracking and evaluation of dendritic cell migration by cellular magnetic resonance imaging. *Wiley Interdiscip Rev Nanomed Nanobiotechnol* 2013; 5: 469–483.
32. Bulte JW and Kraitchman DL. Iron oxide mr contrast agents for molecular and cellular imaging. *NMR Biomed* 2004; 17: 484–499.
33. Siglienti I, Bendszus M, Kleinschnitz C, et al. Cytokine profile of iron-laden macrophages: Implications for cellular magnetic resonance imaging. *J Neuroimmunol* 2006; 173: 166–173.
34. Ahrens ET, Feili-Hariri M, Xu H, et al. Receptor-mediated endocytosis of iron-oxide particles provides efficient labeling of dendritic cells for in vivo mr imaging. *Magn Reson Med* 2003; 49: 1006–1013.
35. He T, Wang Y, Xiang J, et al. In vivo tracking of novel spio-molday ion rhodamine-b-labeled human bone marrow-derived mesenchymal stem cells after lentivirus-mediated cox-2 silencing: A preliminary study. *Curr Gene Ther* 2014; 14: 136–145.
36. Martin A, Aguirre J, Sarasa-Renedo A, et al. Imaging changes in lymphoid organs in vivo after brain ischemia with three-dimensional fluorescence molecular tomography in transgenic mice expressing green fluorescent protein in t lymphocytes. *Mol Imag* 2008; 7: 157–167.
37. Liesz A, Hagmann S, Zschoche C, et al. The spectrum of systemic immune alterations after murine focal ischemia: Immunodepression versus immunomodulation. *Stroke* 2009; 40: 2849–2858.
38. Prass K, Meisel C, Hoflich C, et al. Stroke-induced immunodeficiency promotes spontaneous bacterial infections and is mediated by sympathetic activation reversal by poststroke t helper cell type 1-like immunostimulation. *J Exp Med* 2003; 198: 725–736.
39. Chu HX, Kim HA, Lee S, et al. Immune cell infiltration in malignant middle cerebral artery infarction: Comparison with transient cerebral ischemia. *J Cereb Blood Flow Metab* 2014; 34: 450–459.